First global measurement of midtropospheric CO2 from NOAA polar satellites: Tropical zone

A. Chédin, S. Serrar, N. A. Scott, C. Crevoisier, R. Armante

JOURNAL OF GEOPHYSICAL RESEARCH, VOL. 108, NO. D18, 4581, doi:10.1029/2003JD003439, 2003

First global measurement of midtropospheric CO_2 from NOAA polar satellites: Tropical zone

A. Chédin, S. Serrar, N. A. Scott, C. Crevoisier, and R. Armante

Laboratoire de Météorologie Dynamique, Institut Pierre-Simon Laplace, Ecole Polytechnique, Palaiseau, France

Received 21 January 2003; revised 9 May 2003; accepted 4 June 2003; published 20 September 2003.

[1] Midtropospheric mean atmospheric CO_2 concentration is retrieved from the observations of the NOAA series of polar meteorological satellites, using a nonlinear regression inference scheme. For the 4 years of the present analysis (July 1987 to June 1991), monthly means of the CO_2 concentration retrieved over the tropics (20°N to 20°S) from NOAA 10 show very good agreement with what is presently known. Not only the phase of the seasonal variations (location of the peaks) but also their amplitude and their latitudinal evolution match quite well recent in situ observations made by properly equipped commercial airliners measuring in an altitude range similar to the one favored by the satellite observations. Moreover, the annual trend inferred corresponds to the known increase in the concentration of CO_2 as a result of human activities. Also, the impact of El Niño-Southern Oscillation events is clearly seen and confirms analyses of in situ or aircraft observations and of model simulations. Forty-eight maps of monthly mean midtropospheric CO_2 concentration have been produced at a resolution of $15° \times 15°$. A rough estimate of the method-induced standard deviation of these retrievals is of the order of 3.6 ppmv (around 1%). The coming analysis of the almost 25 years of archive already accumulated by the NOAA platforms should contribute to a better understanding of the carbon cycle. A simulation of the extension of the method to the next generation high-spectral-resolution instruments, with very encouraging results, is presented. *INDEX TERMS:* 0315 Atmospheric Composition and Structure: Biosphere/atmosphere interactions; 0325 Atmospheric Composition and Structure: Evolution of the atmosphere; 0330 Atmospheric Composition and Structure: Geochemical cycles; 1610 Global Change: Atmosphere (0315, 0325); 1640 Global Change: Remote sensing; *KEYWORDS:* satellite observation, carbon dioxide concentration, tropical zone

Citation: Chédin, A., S. Serrar, N. A. Scott, C. Crevoisier, and R. Armante, First global measurement of midtropospheric CO_2 from NOAA polar satellites: Tropical zone, *J. Geophys. Res.*, *108*(D18), 4581, doi:10.1029/2003JD003439, 2003.

1. Introduction

[2] Knowledge of present carbon sources and sinks, including their spatial distribution and their variability in time is essential for predicting future carbon dioxide atmospheric concentration levels. Because the atmosphere integrates over varying carbon surface sources and sinks, the distribution of CO_2 in the atmosphere and its time evolution can be used to quantify surface fluxes. However, this approach is currently limited by the sparse and uneven distribution of the global flask sampling programs. For example, regional carbon budgets are reconstructed from about 100 points. As a consequence, inferring surface sources and sinks from observed concentrations is still highly problematic [*Rayner et al.*, 1999; *Schimel et al.*, 2000].

[3] Satellite measurements of the distribution of global atmospheric CO_2 would in principle fill this gap in scale [*Rayner and O'Brien*, 2001]. Measurements that densely sample the atmosphere, in time and in space, would provide a crucial constraint, allowing uncertainty in transport versus other information (on source and sink characteristics) to be separated and reduced.

[4] Recent studies [*Chédin et al.*, 2002a, 2002b, 2003a] have shown that atmospheric concentration variations (seasonal, annual) of major greenhouse gases (CO_2, N_2O, CO) may be retrieved from observations of the National Oceanic and Atmospheric Administration (NOAA) polar meteorological satellite series, in addition to their main mission of measuring atmospheric temperature and moisture global fields. The method used for these studies was based on the analysis of the differences between the satellite observations and simulations from a radiative transfer model using collocated radiosonde data and fixed gas concentration as the prime input. Its main limit was its dependency upon collocations between satellite observations and radiosonde measurements because of their inability to measure all necessary information (surface temperatures, upper stratospheric temperatures, etc.) and the uneven and, by far, not global distribution of the radiosonde stations.

[5] The method developed here, a nonlinear regression inverse model, relies on the only satellite observations, in essence global. It is applied to the platform NOAA 10,

0148-0227/03/2003JD003439

Table 1. Sensitivities (K) of HIRS Channels to Changes in CO_2 Concentration[a]

Channel	Wavelength, μm	CO_2: +3%
2	14.7	+0.10 ± 0.06
3	14.5	+0.00 ± 0.06
4	14.2	−0.20 ± 0.09
5	14.0	−0.30 ± 0.12
6	13.7	−0.30 ± 0.12

[a]Sensitivities to actual changes (seasonal, interannual) may be deduced linearly.

providing seasonal cycles and trends for latitude bands of 5° and global monthly maps of midtropospheric mean CO_2 concentration, at the spatial resolution of 15° longitude by 15° latitude, for the period July 1987 to June 1991. It may easily be extended to the almost 25 years of archive already accumulated.

2. Satellite Data

[6] The Television and Infrared Operational Satellite-Next Generation (TIROS-N) Operational Vertical Sounder (TOVS) has been flown aboard the National Oceanic and Atmospheric Administration (NOAA) polar meteorological satellites since 1978 [*Smith et al.*, 1979]. This instrument consists of the High-Resolution Infrared Radiation Sounder (HIRS-2), the Microwave Sounding Unit (MSU) and the Stratospheric Sounding Unit (SSU). Scan widths are approximately 2200 km, providing global coverage every 12 hours. HIRS-2 measures atmospheric and/or surface emission in seven channels located around 15.0 μm, five located around 4.3 μm, and an 11.0 μm window channel. Ozone emission is measured in a 9.6 μm channel. Other channels measure water vapor emission around 7 μm and surface emission at shorter wavelengths, around 4 μm. The MSU measures atmospheric emission in four 55-Ghz O_2 channels. In the 15 μm and 4.3 μm spectral bands, measured radiances mostly depend on the temperature of the atmosphere but also on the CO_2 concentration and the concentrations of the other greenhouse gases (N_2O, CO, O_3, in particular). Table 1 lists the mean sensitivities of the channels measuring in the 15 μm spectral domain of absorption of CO_2 to its concentration variation. These numbers were computed from the Automatized Atmospheric Absorption Atlas (4A) model in its latest version [*Scott and Chédin*, 1981; N. A. Scott and A. Chédin, manuscript in preparation, 2003] with up-to-date spectroscopy, using a set of 42 representative atmospheric situations [*Garand et al.*, 2001]. It may be pointed out that stratospheric channels respond positively to an increase of concentration, when tropospheric channels respond negatively. This is due to the slope of the temperature profile.

[7] Retrieving thermodynamic atmospheric and surface variables, like temperature and water vapor profiles or cloud and surface characteristics, goes through the inversion of the radiation transfer equation. The Improved Initialization Inversion (3I) method [*Chédin et al.*, 1985; *Scott et al.*, 1999] was developed at LMD for this purpose and applied, within the framework of the NOAA-National Aeronautics and Space Administration (NASA) Pathfinder program, to the reanalysis of more than 8 years of observations of the platforms NOAA 10, NOAA 11, and NOAA 12. The spatial resolution of the 3I retrievals is a compromise between the spatial resolution of the HIRS and MSU sounders. A 3 × 2 (at the edges of an orbit), or 3 × 3, or 3 × 4 (at nadir) array of HIRS spots is grouped together to form a so-called "3I-box" and then collocated with the nearest MSU spot(s). Such boxes represent a surface of nearly 100 × 100 km^2, and 3I retrievals are performed for each array. Important auxiliary information is stored in each box as the land-sea and day-night flags, the surface elevation, the satellite viewing angle, and the clear-cloudy flag for each HIRS spot. Clouds are detected at the HIRS spatial resolution by a succession of numerous multispectral threshold tests [*Wahiche et al.*, 1986; *Stubenrauch et al.*, 1996, 1999]. An important part of the cloud detection is the use of simultaneous MSU measurements. Since this sounder probes through the clouds, they are used to predict clear-sky infrared brightness temperatures, which are then compared to those observed by the HIRS instrument. Because of its relatively high spectral resolution (compared to imagers), HIRS is very sensitive to cirrus clouds. For example, in the tropics, up to 20% more cirrus than the International Satellite Cloud Climatology Project (ISCCP) are identified by TOVS. This problem is also discussed in section 4.

[8] Contrary to 3I, where a box is declared (and processed as) clear as soon as one of its HIRS spots has been declared clear, here, only boxes having at least 60% of clear HIRS spots are considered as "clear boxes" for the CO_2 retrieval process. Because the viewing angle is limited to approximately 40° to avoid the edges of the orbits, boxes contain either 12 (4 × 3) or 9 (3 × 3) HIRS spots. All clear spots are averaged within each box and CO_2 concentration retrieval is performed for this averaged value.

3. Method

[9] Although the signals induced by the variation of the concentration of CO_2 can clearly be brought into evidence in the observed radiances, they remain weak: a few tenths of a Kelvin as seen in Table 1 [*Chédin et al.*, 2002a, 2003a], and their interpretation in terms of concentration is not straightforward. For that reason, instead of simple linear regressions, we have chosen the more complex way offered by neural network techniques. Here, use is made of the Multilayer Perceptron (MLP) [*Rumelhart et al.*, 1986].

[10] The Multilayer Perceptron (MLP) network is a nonlinear mapping model composed of parallel processors called "neurons." These processors are organized in distinct layers. The first layer represents the input of the mapping. The intermediate layers are called the "hidden layers." These layers are connected via neural links: two neurons i and j between two consecutive layers have synaptic connections associated with a synaptic weight w_{ij}. Each neuron i executes two simple operations. First it makes a weighted sum of its inputs z_i: this signal is called the activity of the neuron:

$$a_i = \sum_{i \in Inputs(j)} w_{ij} z_i \qquad (1)$$

Then, it transfers this signal to its output through a so-called "transfer function," often a sigmoidal function such as

$\sigma(a) = \tanh(a)$. The output z_j of neuron j in the hidden layer is then given by

$$z_j = \sigma(a_j) = \sigma\left(\sum_{i \in Inputs(j)} w_{ij} z_i\right) \quad (2)$$

Given a neural architecture (with specified number of layers, neurons and connections), all the information of the network is contained in the set of synaptic weights $W = \{w_{ij}\}$. The learning algorithm is the optimization technique that estimates the optimal network parameters W by minimizing a positive-definite cost function which measures, for a set of representative patterns for which inputs and outputs are known (the learning set), the mismatch between the neural net outputs and the desired outputs. This enables one to approximate the desired function as closely as necessary by the neural mapping. Here, the Error Back-Propagation algorithm [*Rumelhart et al.*, 1986] is used to minimize the cost function. It is a gradient descent algorithm well adapted to the MLP hierarchical architecture because the computational cost is linearly related to the number of parameters. To avoid being trapped in local minima during the minimization of the cost function, stochastic steepest descent is used. The learning step is made sample by sample, chosen iteratively and stochastically in the learning data set.

3.1. Learning Data Set

[11] Training of the MLPs is performed using the Thermodynamic Initial Guess Retrieval (TIGR) climatological library of about 2300 representative atmospheric situations selected by statistical methods from 80,000 radiosonde reports [*Chédin et al.*, 1985; *Achard*, 1991; *Chevallier et al.*, 1998]. Each situation is described by its temperature, water vapor and ozone profiles (40 levels from 1013 hPa to 0.05 hPa). The ozone profile is specified from the UGAMP ozone climatology [*Li and Shine*, 1995], taking into account the latitude, longitude and time of each situation archived in TIGR. For each atmospheric situation, a surface temperature is generated as the sum of the temperature of the atmosphere at the lowest level and a random number with zero mean and a standard deviation of 4K. Finally, the situations in TIGR are stratified by a hierarchical ascending classification into five air mass types (''tropical''; temperate, ''midlat1''; cold temperate and summer polar, ''midlat2''; Northern Hemisphere very cold polar, ''polar1''; winter polar, ''polar2''), depending on their virtual temperature profiles [*Achard*, 1991; *Chédin et al.*, 1994].

[12] Clear-sky transmittances, brightness temperatures and Jacobians (partial derivatives of the brightness temperature with respect to temperature, gas concentration for H_2O, O_3, CO_2, N_2O and CO, surface temperature and emissivity, etc.) for all TOVS sounding channels are then computed for each situation archived using the fast line-by-line 4A model in its latest version 2000 (N. A. Scott and A. Chédin, manuscript in preparation, 2003). Calculations are performed [*Chédin et al.*, 1985] for 10 viewing angles, between 0° (nadir) and 60° (the maximum value for angular scanning), for 19 values of surface pressure (up to about 500 hPa) for elevated terrains, and for two surface types: land and sea. Over sea, the surface emissivity varies with frequency and viewing angle according to *Masuda et al.* [1988] and *Matricardi and Saunders* [1999]. A fixed emissivity of 0.98 is specified for all channels over land, except for the channels at 4.3 μm, for which the emissivity is 0.97. Minor gas concentrations have been given fixed values, close to the mean values observed during the lifetime of NOAA 10. These values are as follows: 355 ppmv for CO_2, 308 ppbv for N_2O, 1.8 ppmv for CH_4 and 100 ppbv for CO. These results are also stored within the TIGR data set. It is worth pointing out that TIGR is not primarily sensitive to the relative quality of the radiosoundings sampled in it but only to their representativeness and plausibility. In fact, it is sensitive to the quality of the relationship between thermodynamic quantities and radiative quantities. For that reason, great attention has been paid to the validation of the 4A model.

3.2. Training Phase

[13] Temperature is, by far, the variable influencing the most the radiances measured in the so-called ''TOVS CO_2-channels,'' located around 15 μm and 4.3 μm. Greenhouse gases, like CO_2, N_2O or CO, have a significant but minor impact, difficult to separate from the major signal. A good a priori knowledge of the temperature field may, in principle, be retrieved from TOVS. However, the noise associated with these retrievals, at least 1.5 K, makes this information useless for our purpose. In addition, climate-correlated biases associated with retrieved temperatures are particularly difficult to quantify and, thus, to eliminate. Fortunately, the observations made simultaneously by MSU also strongly depend on the temperature, but not on the above greenhouse gas distributions, as measuring in the oxygen microwave band. For these reasons, the predictors selected to enter the training phase must combine HIRS CO_2-sensitive channels and MSU temperature (only)-sensitive channels.

[14] Other important issues for selecting predictors are the capability of the radiative transfer model to simulate them accurately and their low sensitivity to water vapor and other conflicting signals [see *Chédin et al.*, 2003a]. This is the case for the channels considered here.

[15] The composition of the input layer of the MLP (the predictors) follows from the above considerations. For each atmospheric situation of TIGR, the input layer is composed of the following: (1) Brightness temperatures of channels HIRS 4, 5 and 6, the most sensitive to CO_2. The CO_2-Jacobians of these channels peak in the midtroposphere [*Chédin et al.*, 2002a] and, as a whole, approximately integrate the altitude range 4.5–5.0 to about 13 km (see Figure 1). (2) Brightness temperatures of channels MSU 3 and 4, not sensitive to CO_2, but sensitive to temperatures in the midtroposphere. (3) Differences between the brightness temperatures of either MSU 3 or MSU 4 and the HIRS channels 2, 3, 4, and 5, to help teach the MLP about signals influenced by both temperature and CO_2 and signals influenced by the temperature only. It is worth pointing out that the MSU 3 temperature Jacobian (the so-called ''weighting function'') and the mean CO_2-Jacobian for the CO_2 sensitive channels approximately cover the same pressure range (see Figure 1). (4) Brightness temperature of channel HIRS 18, to help constrain the solution for surface temperature, to which channel HIRS 6 is modestly sensitive.

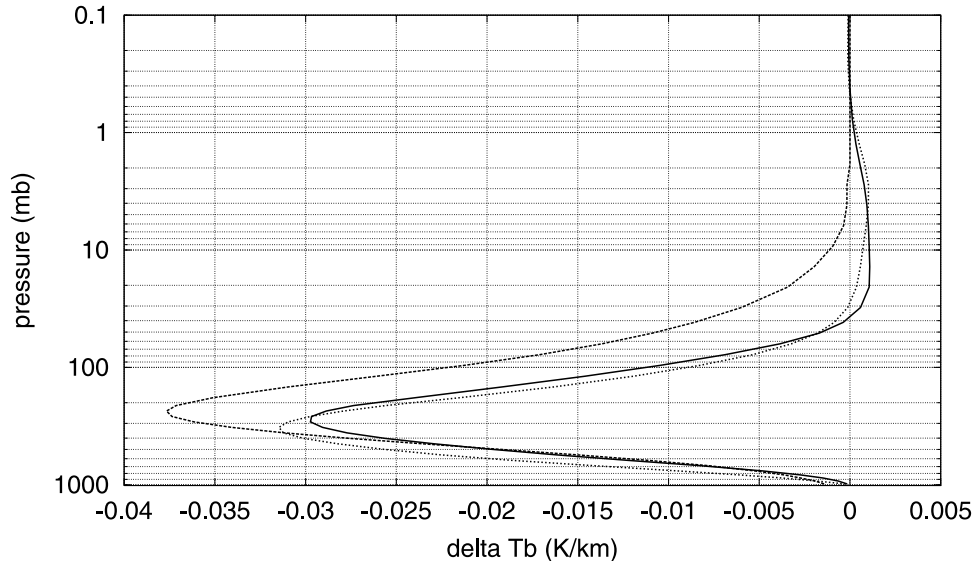

Figure 1. Temperature-Jacobian (weighting function) of channel MSU3 (dashed line, in K/km for an increase of the temperature of 0.5 K) and HIRS mean CO_2 Jacobian of the CO_2 sensitive channels (solid line, in K/km for a 3% increase of the CO_2 concentration). The AIRS mean CO_2 Jacobian is also shown (dotted line, same units).

[16] Altogether, there are 14 entries to the MLP. The output layer (the predictands) is composed of the following: (1) The difference, Δq (ppmv), between the true (associated with inputs) CO_2 concentration value and its reference value (355 ppmv), and (2) the differences, ΔTb, between the true (or input) brightness temperature (with the true value of CO_2) and the reference brightness temperature (with the reference value of CO_2) of channels HIRS 4 and 5, the channels the most sensitive to midtropospheric CO_2, on the other hand.

[17] The ΔTbs, as predictands, play a key role. Because the true and the reference brightness temperatures correspond to the same atmospheric situation (same profiles of temperature, water vapor, ozone, etc.), the only difference being the CO_2 concentration value, they tell the MLP that, to the same Δq, may correspond a variety of ΔTbs resulting from the variety of situations in TIGR. Such a learning process greatly helps to disentangle the CO_2 signal from other conflicting signals and, above all, that of the temperature, but also water vapor, ozone, etc. Because of their reduced temperature variability, the training of the MLP has been limited, for this first attempt, to the 872 atmospheric situations of TIGR belonging to the "tropical" air mass. As a consequence, results presented here are limited to the tropical zone (20°N to 20°S). Our past experience with neural networks and several trials have led us to adopt an MLP with two hidden layers of 50 neurons (first layer) and 30 neurons (second layer).

[18] Input brightness temperatures correspond to randomly drawn values of the CO_2 concentration, in the range 341–369 ppmv. They are computed from the reference values in TIGR using the CO_2 Jacobians. The mean value of 355 ppmv approximately corresponds to the mean concentration of CO_2 over the NOAA 10 time period considered here (July 1987 to June 1991). We have verified that the choice of this "central" value, however within a plausible interval, has a negligible impact on the results. As a consequence, because of the slow evolution of the mean CO_2 concentration, the same network may be used to process data from several satellites (see section 3.3).

[19] Noise equivalent temperature ($NE\Delta T$) is added to the input brightness temperatures in order to account for the instrument and model noises [*Chédin et al.*, 2003a]. Actual instrumental noise values are computed at the temperature of each channel and are divided by the square root of the number of HIRS spots averaged before the retrieval process within each "3I box."

[20] A total of 49 MLPs have been trained, covering 6 surface elevations (from 1013 to 875 hPa) over land and one over sea, and 7 viewing angles (from nadir to about 40°, to avoid the edges of the orbits). Results of the training phase, at the end of the iterative gradient descent process, show no bias and a RMS error of slightly less than 4 ppmv.

3.3. Application to NOAA 10 Observations: Radiation Model Bias Removal

[21] Because the MLPs are trained with simulated data, their application to real data implies that eventual brightness temperature systematic biases between simulations and observations have been eliminated. This may be done by comparing simulations and observations for a set of collocated satellite and radiosonde data. Collocations are from the so-called "DSD5" NOAA/National Environmental Satellite Data and Information Service (NESDIS) collocation archive [*Uddstrom and McMillin*, 1994]. For each channel, the systematic bias is obtained by averaging the difference between simulations and observations over the whole time period considered. It is worth pointing out that removing a constant bias keeps each observation its potential signatures of the variations of CO_2. MSU 3 systematic bias, however, shows a particular behavior over the lifetime of the satellite. Starting, in July 1987, with a value about 0.3 K lower than its mean (simulation minus observation), it increases linearly and reaches a stable constant value by

October–November 1988, up to the end of the period. Similar instrumental problems have already been pointed out for NOAA 6 and NOAA 9 (see Global Hydrology Resource Center User Service at the Internet address http://ghrc.msfc.nasa.gov/uso/readme/userv.html). We have verified that not removing this exceptionally inconstant signature leads to an important excess of CO_2 at the beginning of the time period studied here. This comes from the fact that the HIRS channels give the signal of a correct CO_2 amount and of a correct temperature when MSU 3 gives (from July 1987 to October–November 1988) the signal of too warm an atmosphere (by up to 0.3 K in July 1987). Adding CO_2, with the result of cooling the HIRS channels the most sensitive to CO_2 (tropospheric), is the response of the network to reconcile these somewhat contradictory signals.

[22] Brightness temperature systematic biases are computed separately over sea and over land, for the latitude zone 20°N to 20°S. The well recognized, small but significant, dependence of radiative transfer model errors on the air mass and/or the latitude [*Kelly and Flobert*, 1988; *Uddstrom and McMillin*, 1994; *Chédin et al.*, 2003a] would require analyzing the biases over latitude bands smaller than the above one. However, the too limited number of satellite-radiosonde collocations precludes going much further. Because the retrieved CO_2 concentration may depend on the accuracy of the systematic biases inferred, this difficulty had to be overcome. The solution finally adopted is described in the next section.

[23] Daytime observations are not considered because of possible contamination by solar radiation. As a consequence, with NOAA 10, observations are at around 7:30 pm local time. If the retrieved values are, in general, representative of the mean CO_2 concentration as a result of the smallness of its diurnal cycle at the altitudes observed, there may be regions where it is not the case, for example over tropical forests where the surface diurnal signal can get diluted higher up in the air column by deep convection. Analyzed from the eddy covariance data over tropical forests (http://www-eosdis.ornl.gov/FLUXNET/), a maximal surface diurnal cycle amplitude of the flux of 3000 gC m^{-2} y^{-1}, if instantaneously mixed over an air column of 10 km, would generate a diurnal cycle in the atmospheric column of 2 ppmv (P. Ciais, private communication, 2003). Indeed, *Wofsy et al.* [1988], carrying out frequent aircraft vertical profiles of CO_2 over the Amazon basin, measured a diurnal cycle amplitude of the order of 2–3 ppmv that is present in the atmosphere up to at least 4 km.

4. Results and Comparisons With Aircraft Observations

[24] Four years of NOAA 10 observations (from July 1987 to June 1991, inclusive) have been processed and interpreted in terms of midtropospheric CO_2 concentration. For reasons given in section 3.2, the part of the globe covered by the present study has been limited to 20°N to 20°S. It is worth pointing out that it coincides with the region where the surface flask network is the least efficient and, also, with the region of strong convective vertical mixing which rapidly transmits surface carbon flux variations to that part of the troposphere observed by the satellite.

[25] The initial basic resolution is one day (one observation of NOAA 10 at about 7:30 pm local time) and 1° longitude by 1° latitude. This elementary retrieval will be referred to as "one item" in the following. Items are then grouped together on a monthly basis within zonal latitude bands of 1° each, between 20°N and 20°S. For each such group of items (monthly, 1° latitude band), possible remaining cloud interferences are then accounted for through a 1.3 sigma (sigma being the standard deviation of the item sample) elimination procedure, leaving 80% of the original sample.

[26] Although very efficient (see section 2), the TOVS/3I cloud-screening scheme may fail to detect very thin cirrus, particularly those appearing near the tropical tropopause [*Winker and Trepte*, 1998; *Hartmann et al.*, 2001]. They extend several hundred to more than a thousand kilometers and persist for time periods of several hours to more than a day before dissipating. Such clouds, which may potentially adulterate the retrieval of the CO_2 concentration, are the main targets of this simple statistical elimination procedure. Tropopause cirrus occur frequently above convective anvil clouds. *Wang et al.* [1998] showed that approximately 30% of the Stratospheric Aerosol and Gas Experiment (SAGE) II cloud measurements are isolated single-layer clouds, while 65% are high clouds contiguous with an underlying opaque cloud. If the latter category is detected through the underlying opaque cloud, the former category may be more problematic for the retrieval of CO_2. However, *Winker and Trepte* [1998], analyzing Lidar In-space Technology Experiment (LITE) observations, find a cloud fraction of "laminar" cirrus (physical depth less than 1 km) of 14% within the latitude band 30 N to 20 S. Associating these results from SAGE II and LITE leads to quite low a percentage of occurrence of very thin, isolated and possibly undetected, clouds. Simulations carried out using microphysical and radiative properties typical of the tropopause cirrus observed and the parameterization of *Fu et al.* [1998] for nonspherical particles, show that clouds with optical depths as low as 0.05 at 14 μm (a value close to that at 0.55 μm) are generally detected (computation made with particles having an effective diameter of 20 μm; smaller particles, actually observed, would lead to smaller an optical depth threshold). It may be reasonably expected that most of the radiance contamination from remaining, undetected, clouds is largely diluted by the space (15°) and time (1 month) averaging used to produce mean CO_2 concentrations (see below). It is also worth pointing out that the background contamination (mean over the geographical area and time period considered) is removed by the radiation model bias removal procedure (see section 3.3). Only long lasting and extended episodes of contamination by undetected very thin cirrus, quite unlikely to happen according to present observations, could result in erroneous retrievals of the concentration of CO_2.

[27] Results are shown either zonally, for latitude bands of 5°, for the purpose of comparison with existing aircraft observations (see below), or globally, at the resolution of 15° latitude by 15° longitude, chosen in such a way that enough items are present in each grid box to give robust

Table 2. Zonal Means Over the Period July 1987 to June 1991 of the CO_2 Concentration Given by *GLOBALVIEW-CO_2* [1999] and As Retrieved From NOAA 10, for 5° Latitude Bands From 20°N to 20°S[a]

Latitude Band	GLOBALVIEW (*a*)	NOAA 10 (*b*)	Difference (*a* − *b*)
20°–15°N	353.3	353.5	−0.2
15°–10°N	353.3	353.6	−0.3
10°–5°N	353.3	353.1	+0.2
5°N to EQ	353.1	352.6	+0.5
EQ to 5°S	352.9	352.5	+0.4
5°–10°S	352.4	352.5	−0.1
10°–15°S	351.8	352.6	−0.8
15°–20°S	351.5	353.7	−2.2

[a]Values are given in ppmv.

statistics. A grid box with less than 300 items, indicating an area where dense cloudiness dominates, is rejected (see section 4.4).

4.1. CO_2 Concentration Bias Removal

[28] A first examination of the initial monthly maps of CO_2 concentration (not shown) retrieved using the method described in section 3 has brought into evidence small, but significant, latitudinal discontinuities. They may be approximately quantified by comparing zonal means of CO_2 concentration, averaged over the period of 4 years considered here, obtained either from NOAA 10 or from the *GLOBALVIEW-CO_2* [1999] (also available on Internet via anonymous FTP to ftp.cmdl.noaa.gov, path ccg/co2/GLOBALVIEW) data set, itself primarily made of ground-based in situ observations. Table 2 presents this comparison for latitude bands of 5° from 20°N to 20°S. These discontinuities are essentially due to the insufficient accuracy of the determination of the radiative transfer model brightness temperature systematic biases and, in particular, of their dependence with latitude (see section 3.3). These differences are found smaller for the latitude bands where the corresponding number of collocations is larger. The band 15°–20°S, with a mean bias of 2.2 ppmv is, by far, the worse case. To remove these discontinuities, each retrieval is being added the difference value of column 4 of Table 2 corresponding to its latitude. Doing so makes the mean values of all the retrievals within a given 5° latitude band over the 4 years equal to the corresponding mean value of the *GLOBALVIEW-CO_2* [1999] data set. This adjustment implies that the mean of the CO_2 concentration over the 4 years considered is the same at the surface and averaged over the altitude range seen by the satellite. This adjustment is fully reversible and easy to correct and improve.

4.2. Seasonal Cycle and Trend (Zonal Means)

[29] Our knowledge of the distribution of CO_2 in the middle to high troposphere is quite limited at present. However, two studies [*Matsueda et al.*, 2002; *Nakazawa et al.*, 1991] cover relatively long periods of time and relatively wide domains of latitude. *Matsueda et al.* [2002] (hereinafter referred to as MII) report on in situ observations made twice a week from commercial airliners. These measurements go from April 1993 to April 1999 and were made within the altitude range 9–13 km and extend in latitude from 30°N to 30°S, between Japan and Australia. In 1984 and 1985, similar observations made between Tokyo and Anchorage, and between Tokyo and Sydney, were analyzed by *Nakazawa et al.* [1991]. Figure 8 of MII shows the mean observed seasonal cycle for 12 latitude bands of 5° each, between 30°N and 30°S. It may be directly compared to our Figure 2, which displays similar cycles, retrieved from NOAA 10 between 20°N and 20°S. The agreement is relatively good for what concerns both the amplitudes and the phases of the cycles: rapid decay of the amplitude from 20°N to the equator and delay of phase. Similarly, both sources of data show a more complex Southern Hemisphere seasonality, also pointed out by *Nakazawa et al.* [1991], with two concentration peaks: around June–July and November–December for the aircraft observations, and around May and November for the satellite retrievals. This one-month lag may be explained by the fact that the altitude ranges observed are different: from 9 to 13 km for in situ observations and from 4.5–5.0 to about 13 km for NOAA 10

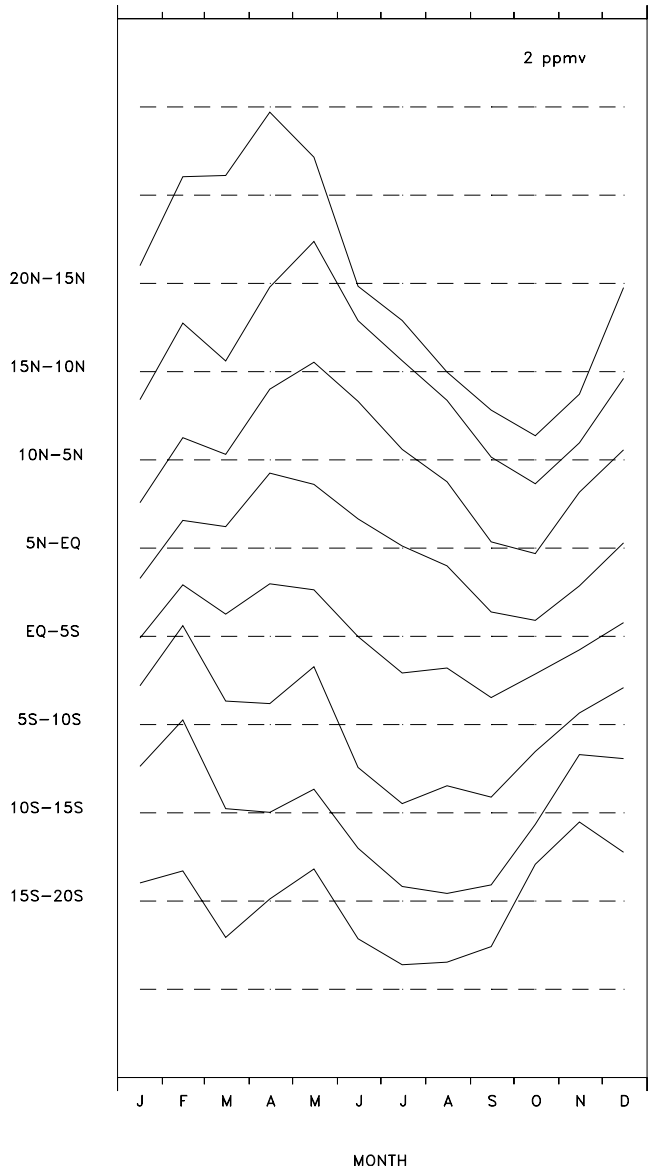

Figure 2. Mean seasonal cycle for 8 latitude bands between 20°N and 20°S as retrieved from NOAA 10 (July 1987 to June 1991); mean altitude range covered ~4.5–5.0 to 13 km. Ordinate division length is 2 ppmv.

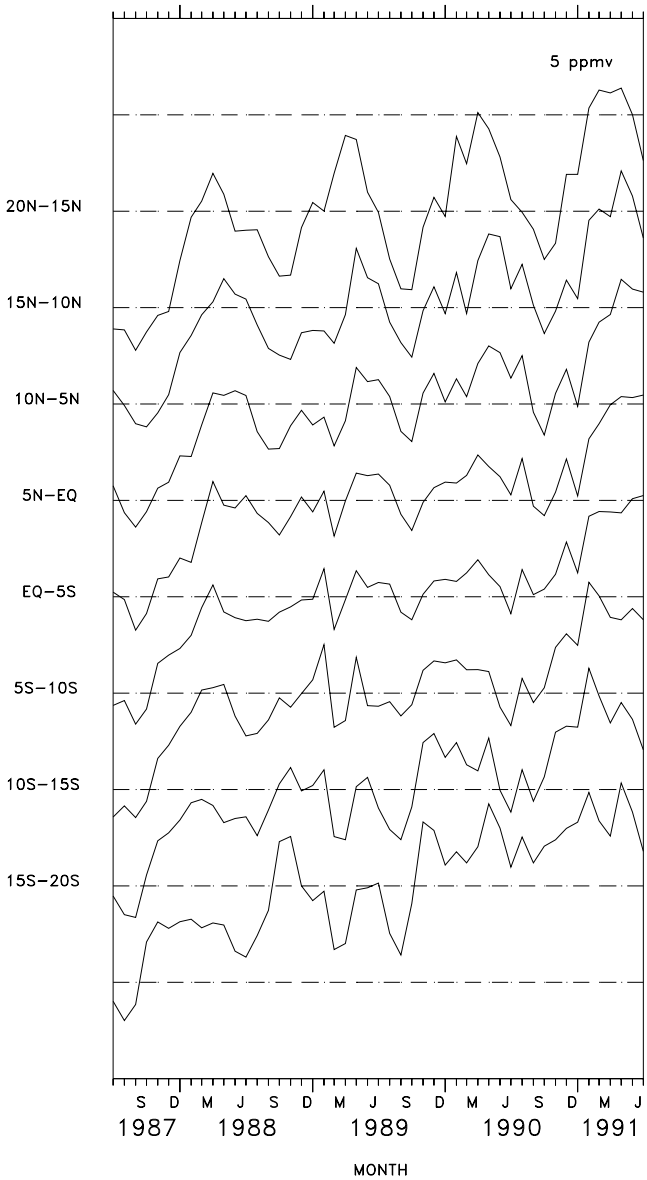

Figure 3. Time variation (monthly means) of the CO_2 concentration for 8 latitude bands between 20°N and 20°S as retrieved from NOAA 10 for the period July 1987 to June 1991. Ordinate division length is 5 ppmv.

[*Nakazawa et al.*, 1991, 1992]. Figure 2 also shows peak-to-peak amplitudes of the average seasonal CO_2 cycles slightly larger than those shown in Figure 8 of MII, in agreement with the above references. Because Figure 8 of MII integrates the longitudes between 140°E and 160°E, when our Figure 2 integrates all longitudes, we have verified that these conclusions also apply to our retrievals when restricted to the same longitude range.

[30] Figure 3 shows the time variation (monthly means) of the CO_2 concentration for the same 8 latitude bands of 5°, from 20°N to 20°S, and from July 1987 to June 1991. These results are in good coherence with the observations reported by MII in their Figure 3. Time variations are clearly seen as mostly seasonal for the northern latitudes and become gradually more complex as going southward. Year-to-year changes are also seen and might reflect the fact that the time period covered starts with the influence of the (declining) 1986–1987 El Niño, continues with the 1988–1989 strong La Niña, to end with the beginning of the 1991 El Niño.

[31] Further analysis of the data of Figure 3 is carried out following a procedure similar to *Matsueda and Inoue* [1996] or to *Duglokencky et al.* [1994]. First, for each latitude band, the average long-term trend and seasonal cycle are approximated by fitting the sum of a first-order polynomial and four harmonics (to account for the complexity of the seasonal cycle) to the data:

$$f(t) = a_1 + a_2 t + \sum_{i=1}^{4} [a_{2i+1} \sin(2\pi i t) + a_{2i+2} \cos(2\pi i t)] \qquad (3)$$

[32] Second, to account for interannual variations in the trend, the differences between the fitting curve of equation (3) and the data (the residuals) are smoothed by applying a low-pass filter (Hann window) that excludes variations occurring on timescales of less than 1 year. The result is added to the linear portion of equation (3) to obtain a (deseasonalized) trend function F(t) [*Duglokencky et al.*, 1994].

[33] Figure 4 summarizes the results of this analysis for the northern tropics (0°–20°N; Figure 4a) and for the southern tropics (0°–20°S; Figure 4b). In each figure, the crosses are for the individual (monthly mean) retrievals;

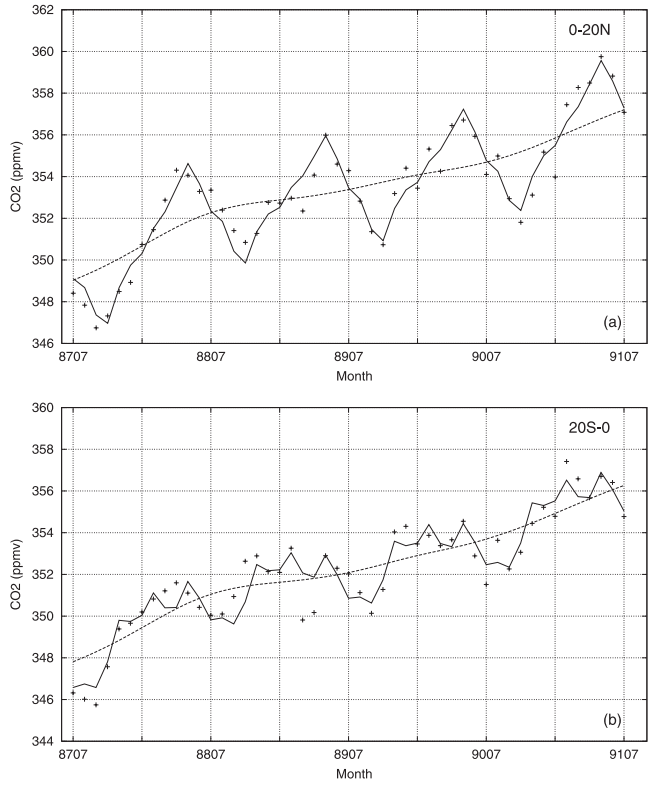

Figure 4. Time variations of CO_2 concentration for (a) the northern tropics (0°–20°N) and (b) the southern tropics (0°–20°S). The crosses represent the individual (monthly mean) data. The dashed line represents the long-term trend (function F(t), see text), and the solid line represents the sum of the trend and the harmonics.

the dashed line is the trend function F(t) and the solid line is the sum of F(t) and the harmonics. On the whole, the fit is good, with no bias and a standard deviation of 0.67 ppmv for the northern tropics and 0.74 ppmv for the southern tropics where the seasonal cycle is more complex. A few points remain relatively far from the fit, for example March 1989 or January 1991 for the northern latitudes, or October 1988 and March–April 1989 (which present the largest departures), for the southern latitudes. A large part of these few significant discrepancies may probably be explained by the seasonally varying spatial distribution of the items (individual CO_2 retrieval), which follows that of clear sky. We have verified that the monthly item spatial distribution closely follows that of the distribution of the clouds as seen, for example, by TOVS [*Scott et al.*, 1999] or by the ISCCP cloud maps available via Internet at the address http://isccp.giss.nasa.gov/zproducts/onlineData.html. The larger the number of items, the smaller the monthly mean cloud amount. Averaging over a particular spatial distribution of the items, having in mind not only the latitudinal (see below), but also the meridional natural CO_2 distribution may lead to an ''anomalous'' value. Taking into account the fact that the time period considered is marked by a number of natural events caused by the El Niño-Southern Oscillation (ENSO), with a series of El Niño and La Niña, such remaining discrepancies might also be due to ''anomalous'' true values of the CO_2 concentration. A detailed analysis of these out-of-fit months is presently being undertaken, and will include the potential (although probably small) influence of the biomass burning [MII; *Duncan et al.*, 2003].

4.3. Growth Rates

[34] Figure 5 shows the time variation of the CO_2 growth rates for the above mentioned 8 latitude bands obtained from the time derivative of the trend function F(t) associated with each band. Similar patterns are observed, however with significant interannual variations around a mean value of 1.75 ppmv/year, over the time period considered, a value very close to the one observed at the surface [*Conway et al.*, 1994]. The two most common features are a sharp decrease of the growth rate at the beginning of the period, down to a minimum value appearing in December 1988 to January 1989 for the deep tropics and a bit later when going northward or southward, and a more or less rapid increase at the end of the period, starting in March–April 1990 for the deep tropics and significantly later for the more northern and (especially) southern latitudes. A secondary maximum is observed in September 1989 for the northern latitudes and in October 1989 for the southern latitudes, and is less pronounced for the deep tropics.

[35] Figure 6a shows the mean growth rates for the northern (0°–20°N) and the southern (0°–20°S) tropics and emphasizes the previously observed patterns, and, at the same time, draws attention to the relationship between the rate of rise of CO_2 and the ENSO [*Bacastow*, 1976; *Keeling et al.*, 1995; *Feely et al.*, 1999; *Jones et al.*, 2001]. Figure 6b shows the Southern Oscillation Index (SOI) monthly means from NOAA/National Centers for Environmental Prediction (NCEP) website (http://www.cpc.ncep.noaa.gov/products/), for the time period considered. The dashed line is the 7-month running mean as in MII. The correlation between the CO_2 growth rate and the SOI is obvious and very similar to the correlation observed by MII, although the time period is different. La Niña events clearly correspond to a decrease of the growth rate and the contrary for El Niño events. More precisely, as shown by *Jones et al.* [2001], the terrestrial biosphere becomes a net source of CO_2 to the atmosphere during El Niño events and the opposite happens for La Niña events. It is the contrary for the ocean. However, the land response being of larger magnitude than that of the ocean, the overall result is an increase of atmospheric CO_2 during El Niño events and the reverse for La Niña years. Figure 6c, similar to Figure 5 of MII, shows the relationship between the CO_2 monthly mean growth rates and the SOI, the plus signs being for the northern tropics and the

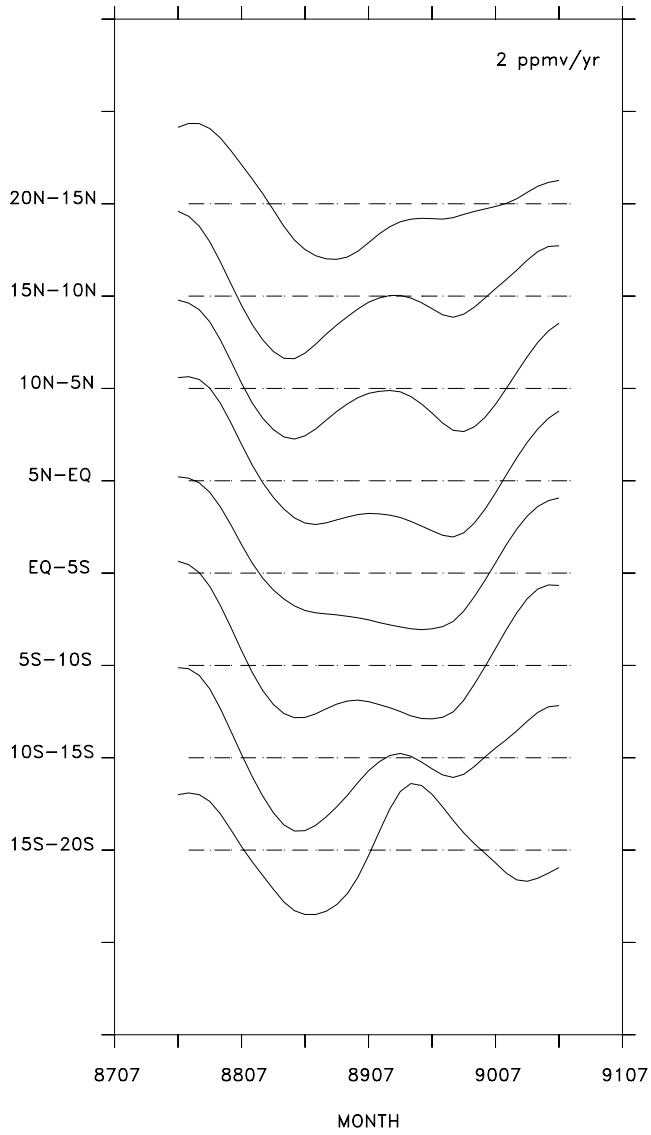

Figure 5. Time variations of the CO_2 growth rate for 8 latitude bands from 20°N to 20°S as retrieved from NOAA 10 over the time period July 1987 to June 1991. Ordinate division length is 2 ppmv/yr.

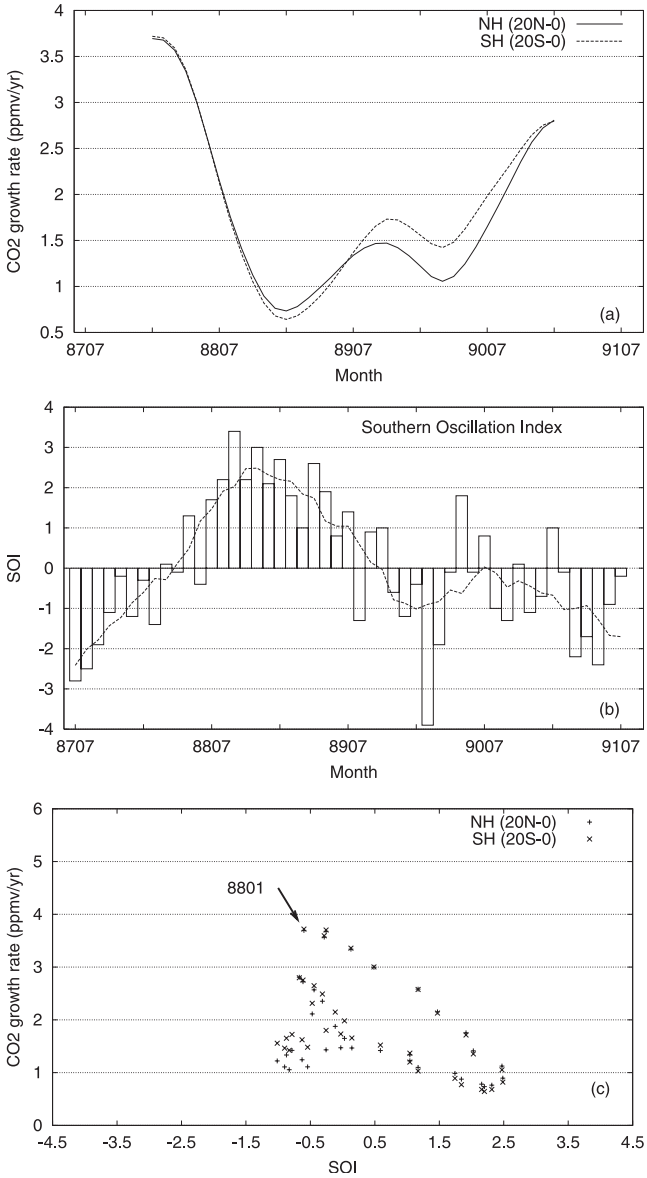

Figure 6. (a) Time variation of the CO_2 growth rate for the northern tropics (0°–20°N), solid line, and for the southern tropics (0°–20°S), dashed line, as retrieved from NOAA 10; (b) time variation of the Southern Oscillation Index (SOI) and its 7-month running mean, dashed line; (c) relationship between the CO_2 growth rate and the SOI for the northern tropics, plusses, and for the southern tropics, crosses.

crosses for the southern tropics. Each cross represents one month and the time sequence starts from the upper left crosses, the first month being here January 1988. The relationship appears most significant when the SOI values are not too close to zero, which is not surprising, and appears mostly noisy when it is the case. The upper part of the sequence corresponds to the decrease of the growth rate, itself associated with the decline of the 1986–1987 El Niño and the development of the 1988–1989 La Niña, and the lower part to the overall increase of the growth rate, consequence of the decline of the La Niña event and of the arriving El Niño of 1991. The relationship observed by MII presents numerous similarities (see their Figure 5), with almost the same slope. The differences, in particular the bi-modal behavior seen in Figure 6c, contrary to Figure 5 of MII, may probably be attributed to the differences between the two time periods studied. Altogether, the conclusions obtained here almost completely agree with those of MII.

[36] Figure 7 shows the latitudinal dependence of the CO_2 concentration, obtained from the eight 5° latitude bands between 20°N to 20°S, separately for the 4 years of the present study. The first year is July 1987 to June 1988, etc. The mean north to south decreasing trend clearly seen in this figure follows from the CO_2 bias removal procedure described in section 4.1. However, because this procedure relies on 4-year averaged zonal means, it is interesting to see how each year evolves separately from the other three. First, the two years 1987–1988 and 1988–1989, marked by ENSO events of opposite signs, display latitudinal patterns that are similar in the southern tropics, with a relatively large decreasing trend, and opposite in the northern tropics, with a weak maximum around 10°N for 1987–1988 (declining El Niño) and a minimum at the same latitude for 1988–1989 (La Niña). MII find a weak maximum around 10°N for non-El Niño years, but, as already pointed out, the time period they study is not marked by a strong La Niña event as it is the case here. The two last years are similar, with a smaller decreasing trend, particularly in the southern tropics. These conclusions are mostly similar to the ones of MII but not identical. Moreover, it must be kept in mind that the NOAA 10 retrievals are influenced by atmospheric layers lower than the ones observed by MII. Finally, the rate of rise of the first year is, as expected, significantly larger than the other two, as a result of the impact of the 1986–1987 El Niño.

4.4. Global Maps of Midtropospheric CO_2 Concentration

[37] Forty-eight maps of monthly mean midtropospheric CO_2 concentration (gross average between 4.5–5.0 to 13 km), covering the period from July 1987 to June 1991, have been produced at the spatial resolution of 15° × 15° (1° × 1° moving average). The choice of this spatial resolution results from a compromise between two requirements of having a relatively dense spatial coverage

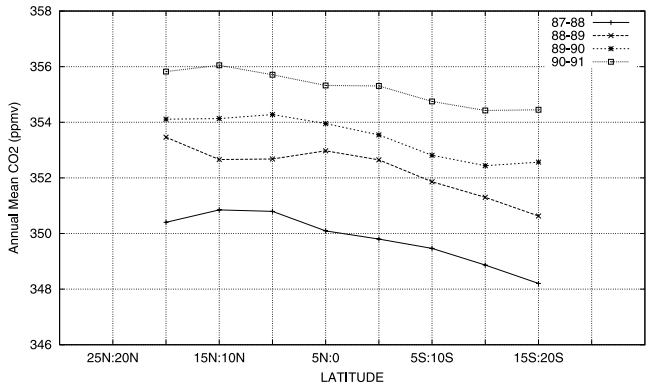

Figure 7. Latitudinal distribution of annual mean CO_2 concentration during 1987–1991 as retrieved from NOAA 10. The year "87–88" means July 1987 to June 1988.

(increasing the spatial resolution) and obtaining robust statistics (decreasing the spatial resolution). Monthly statistics for a grid box of 15° × 15°, having in mind that the elementary retrievals are done daily and at 1° × 1° (one item) boxes, with a climatological cloud coverage of 70%, correspond to a maximum number of items of 2025. Actually, the real number of items greatly varies around this mean value, from about 2000 for areas where clear-sky situations dominate, to below 100, for highly convective areas. A requirement of at least 300 items in a box has been considered as necessary to produce sufficiently robust statistics while not opening too big gaps with no retrievals on the maps.

[38] A first way of quantifying the dispersion of the retrievals, in the absence of observed global maps of the CO_2 concentration, is to determine the standard deviation of each monthly 15° × 15° box item sample. A rather small dispersion around a mean value of 4.2 ppmv is observed (1.2% of the mean CO_2 concentration), a relatively low value, partly explained by the errors due to the method and to the instrument, with its limited capabilities, and partly by the natural variability of CO_2 within each box over one month. The smallest values of the standard deviation (3.6–3.8 ppmv) correspond to the months of July–September where the natural variability (and the concentration, in particular in the northern tropics) is at its minimum, and the maximum values (4.6–4.8 ppmv, at the exception of the La Niña Spring 1989, with values of 4.8–5.0 ppmv) correspond to the months of February–April where the natural variability (and the concentration, in particular in the northern tropics) is at its maximum. These standard deviations may tentatively be seen as resulting from the combination of the standard deviation of the method (σ_M) itself and of the standard deviation of the natural variability (σ_V) of CO_2 (15° × 15°, one month). Doing so, σ_M comes to about 3.6 ppmv (close to 1%) and σ_V comes to 1 ppmv in July September and to less than 3 ppmv in February–April. Such numbers look reasonable. However, this result is more an appreciation of the internal consistency of the method than an estimation of its accuracy. Associated with the comparison to in situ aircraft measurements, it brings some confidence in the overall description of the gross features of the CO_2 field variability.

[39] Figure 8 shows the results obtained for 4 months of August (1987–1990), corresponding to a low CO_2 concentration variability, and 4 months of March, corresponding to a high variability. The time period considered being marked by a series of ENSO events, the four months of March and the four months of August show large interannual variations. Both series also clearly show the mean increase of the CO_2 concentration with time. Gaps due to clouds, although partly masked by the 1° × 1° moving average procedure, mostly follow the regions of deep convection. For the months of August, the region of higher concentration of CO_2 appears rather equatorial, over both land and sea. The variability is minimal over the Pacific Ocean and maximal over the Indian Ocean. For the months of March, as expected, the higher variability is in the northern tropics. The western Pacific appears less variable than the eastern Pacific. The contrast is important between the northern and the southern tropics. A more complete analysis of these retrievals should go through their interpretation in terms of surface fluxes via a carbon flux inversion model coupling in situ and space observations (in progress in co-operation with the Laboratoire des Sciences du Climat et de l'Environnement, Saclay, France, and the Max-Planck Institute for Biogeochemistry, Jena, Germany).

5. Extension of the Method to the Next Generation High-Spectral-Resolution Instruments

[40] Following NOAA/TOVS, a new generation of satellites such as NASA/Aqua, launched in May 2002, or EUMETSAT/MetOp scheduled for 2005, will fly instruments that should improve our capability to monitor CO_2 and other trace gases from space. In particular, now flying onboard Aqua, the Atmospheric Infrared Sounder (AIRS) measures 2378 frequencies at high spectral resolution and covers most of the infrared spectrum while the Advanced Microwave Sounding Unit (AMSU-A) measures 15 microwave frequencies. The method developed in section 3 has been extended to the processing of AIRS/AMSU channels.

[41] First, a set of 43 AIRS channels presenting the best properties to retrieve CO_2 atmospheric concentrations is selected [*Crevoisier et al.*, 2003]. The corresponding mean CO_2 Jacobian, similar to that of TOVS, but peaking slightly lower, is shown in Figure 1. Second, as for TOVS, a two hidden layers MLP is used. Its input layer is made of the brightness temperatures of the 43 AIRS channels selected, 4 window channels (2 in the 4.3 μm band and 2 in the 15 μm band) constraining the solution for surface temperature, and 10 AMSU channels (channels 5 to 14). The output layer is composed of the difference Δq (ppmv), between the true and the reference values of the CO_2 concentration, and of the 43 AIRS ΔTb. The hidden layers are made of 104 and 44 neurons. As for TOVS, the learning data set is made of the TIGR atmospheric situations associated with the corresponding brightness temperatures and Jacobians for each AIRS channels, computed using the 4A model, and assuming fixed values for trace gases concentrations: 372 ppmv for CO_2, 324 ppbv for N_2O and 100 ppbv for CO. These are the predicted concentration values for the year 2003 [*Intergovernmental Panel on Climate Change* (*IPCC*), 1995].

[42] Input brightness temperatures correspond to randomly drawn values of the CO_2 concentrations in the range of 352–392 ppmv. Nominal noise equivalent temperature is added to the input brightness temperatures. The training is made, at present, for a single surface elevation (1013 hPa) and a single viewing angle (nadir).

[43] Trained on the 872 TIGR tropical situations, RMS error on the concentration is 1.7 ppmv. As expected, this value is much lower than the 4 ppmv obtained for TOVS.

[44] Trained on the 742 TIGR temperate situations, the results show no bias and an RMS error of 2.0 ppmv, a value greater than with the tropical situations because of the higher temperature variability of the temperate situations, making the CO_2 signal less independent from the temperature field than for the tropical situations. However, the value reached is good and leaves great hope for the retrieval of CO_2 concentration in temperate zone.

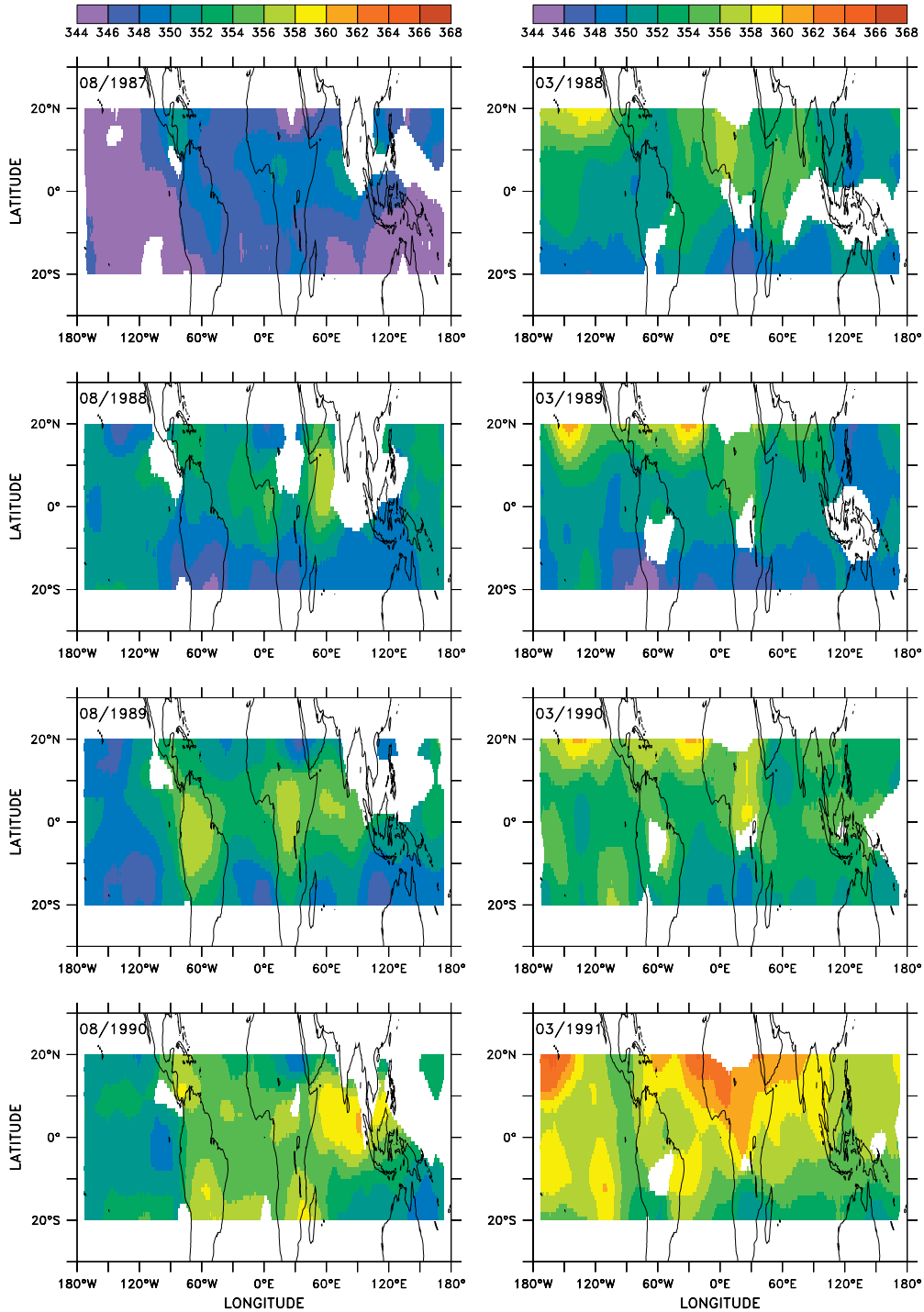

Figure 8. CO_2 monthly mean concentration maps as retrieved from NOAA 10, at a resolution of $15° \times 15°$ ($1° \times 1°$ moving average), for four months of August (1987–1990), for which the CO_2 concentration variability is minimal (left), and four months of March, for which the CO_2 concentration variability is maximal (right). For both series, the regular increase of the mean CO_2 concentration is clearly seen.

[45] Real AIRS and AMSU data are now becoming available at LMD and are about to be processed and interpreted in terms of global maps of CO_2 concentration.

6. Conclusion and Perspectives

[46] Recent studies [*Chédin et al.*, 2002a, 2002b, 2003a] have shown that signatures of the atmospheric concentration variations of major greenhouse gases and, in particular, CO_2, may be detected from the observations made by the NOAA polar meteorological satellites, in addition to the main signatures of atmospheric temperature, moisture, surface or cloud characteristics. The CO_2 signatures, which essentially come from the middle to high troposphere, are weak and not easy to interpret in terms of global fields of CO_2 concentration. The method developed in this article, a

nonlinear regression inference scheme based on the Multilayer Perceptron (MLP), has proven its ability to retrieve important features of the distribution of CO_2 and of its time evolution. The period covered goes from July 1987 to June 1991 and the observations are from NOAA 10. The area analyzed has been, in a first step, restricted to the tropics (20°N to 20°S) where the lower variability of the atmospheric temperature helps to decorrelate its variations from those of CO_2. In almost complete agreement with accurate, middle- to high-tropospheric in situ measurements made by properly equipped commercial aircrafts over a long period of time (see MII), satellite retrievals are able to (1) describe the CO_2 seasonal cycle and its evolution in latitude; (2) describe the time variation of the CO_2 concentration as a function of latitude; (3) quantify the mean rate of rise of CO_2 over the 4-year period (a value of 1.75 ppmv/year is found) and describe the time evolution of the CO_2 growth rate as a function of latitude; (4) confirm the strong correlation between the growth rate and the Southern Oscillation Index (SOI) during a time period marked by the declining 1986–1987 El Niño, the strong 1988–1989 La Niña, and the coming 1991 El Niño; and (5) produce monthly mean global maps of midtropospheric CO_2 concentration at a resolution of 15° by 15°. Within each such grid-boxes, the standard deviation of the sample of CO_2 retrievals, after having deduced an estimate of the part attributed to the natural variability of CO_2 over one month, is of the order of 3.6 ppmv, close to 1%.

[47] The main limit of the method developed here is the dependence of the retrievals on the capability of the forward radiative transfer model, used to create the MLP training data set, to accurately match the satellite observations. Any such model has biases that are air mass, and possibly latitude, dependent. Removal of these biases goes through the use of large sets of collocated radiosonde (to feed the forward model) and satellite observations. Problems arise when latitude bands are not enough covered by such "match-ups." This is the case here, in particular for the latitude band 15°–20°S and, much worse, 20°–25°S (not shown). This is the reason for which this procedure has been complemented by a (fully reversible) retrieval-bias removal procedure relying on 4-year averages of 5° zonal means of the CO_2 concentration from the *GLOBALVIEW-CO_2* [1999]. Using this modest a priori information, made of a total of 8 numbers (one for each latitude band of 5°), has almost no impact on the conclusions drawn by this study. However, to get rid of this information and to refine our knowledge of the forward radiative transfer model systematic biases, great efforts are presently being made to augment the collocation files from the European Center for Medium Range Weather Forecasting (ECMWF) ERA-40 archive.

[48] Fortunately quite unlikely to happen, long-lasting and extended episodes of contamination by very thin cirrus (optical depth at 14 μm less than 0.05) could also be a problem and result in erroneous retrievals of the CO2 concentration (artificial increase by a few ppmv).

[49] The planned analysis of the almost 25 years of archive already accumulated by the NOAA polar platforms should certainly contribute to a better understanding of the carbon cycle through the interpretation of these retrievals in terms of surface carbon fluxes via a carbon flux inversion model, coupling in situ and space observations.

[50] These results also strengthen our hope of greatly improving our knowledge of the global distribution of a variety of radiatively active gases with coming second-generation vertical sounders like AIRS or IASI, both characterized by a much higher spectral resolution allowing a more sophisticated retrieval scheme than the one developed here for the present TOVS channels [*Chédin et al.*, 2003b] and a still better handling of the cloud detection. The first simulations obtained with a similar retrieval method presented in this paper are extremely encouraging.

[51] **Acknowledgments.** This work has been supported by the European Community, under contract EVG1-CT-2001-00056 (the project "COCO"), and by CNRS, CNES, and Ecole Polytechnique. We have also benefited from the large facilities of IDRIS, the computer center of CNRS. We are happy to thank P. Ciais, A. Hollingsworth, C. Pierangelo, and C. Stubenrauch for their help and for fruitful discussions. Warm thanks are also due to the two anonymous referees for their particularly constructive and helpful comments and criticism.

References

Achard, V., Trois problèmes clés de l'analyse 3D de la structure thermodynamique de l'atmosphère par satellites. Thèse de doctorat, Univ. Paris 7, 168 pp., 1991.

Bacastow, R. B., Modulation of atmospheric carbon dioxide by the Southern Oscillation, *Nature*, *261*, 116–118, 1976.

Chédin, A., N. A. Scott, C. Wahiche, and P. Moulinier, The improved initialisation inversion method: A high resolution physical method for temperature retrievals from satellites of the TIROS-N series, *J. Clim. Appl. Meteorol.*, *24*, 128–143, 1985.

Chédin, A., N. A. Scott, C. Claud, B. Bonnet, J. Escobar, S. Dardaillon, F. Cheruy, and N. Husson, Global scale observation of the Earth for climate studies, *Adv. Space Res.*, *14*(1), 155–159, 1994.

Chédin, A., S. Serrar, R. Armante, N. A. Scott, and A. Hollingsworth, Signatures of annual and seasonal variations of CO_2 and other greenhouse gases from NOAA/TOVS observations and model simulations, *J. Clim.*, *15*, 95–116, 2002a.

Chédin, A., A. Hollingsworth, N. A. Scott, S. Serrar, C. Crevoisier, and R. Armante, Annual and seasonal variations of atmospheric CO_2, N_2O and CO concentrations retrieved from NOAA/TOVS satellite observations, *Geophys. Res. Lett.*, *29*(8), 1269, doi:10.1029/2001GL014082, 2002b.

Chédin, A., S. Serrar, A. Hollingsworth, R. Armante, and N. A. Scott, Detecting annual and seasonal variations of CO_2, CO and N_2O from a multi-year collocated satellite-radiosonde data-set using the new Rapid Radiance Reconstruction Network (3R-N) model, *J. Quant. Spectrosc. Radiat. Transfer*, *77*, 285–299, 2003a.

Chédin, A., R. Saunders, A. Hollingsworth, N. A. Scott, M. Matricardi, J. Etcheto, C. Clerbaux, R. Armante, and C. Crevoisier, The feasibility of monitoring CO_2 from high-resolution sounders, *J. Geophys. Res.*, *108*(D2), 4064, doi:10.1029/2001JD001443, 2003b.

Chevallier, F., F. Cheruy, N. A. Scott, and A. Chédin, A neural network approach for a fast and accurate computation of a longwave radiative budget, *J. Appl. Meteorol.*, *37*, 1385–1397, 1998.

Conway, T. J., P. P. Tans, L. S. Waterman, K. W. Thoning, D. R. Kitzis, K. A. Masarie, and N. Zhang, Evidence for interannual variability of the carbon cycle from the National Oceanic and Atmospheric Administration/Climate Monitoring and Diagnostics Laboratory global air sampling network, *J. Geophys. Res.*, *99*, 22,831–22,855, 1994.

Crevoisier, C., A. Chédin, and N. A. Scott, AIRS channel selection for CO_2 and other trace gases retrieval, *Q. J. R. Meteorol. Soc.*, in press, 2003.

Duglokencky, E. J., K. A. Masarie, P. M. Lang, P. P. Tans, L. P. Steel, and E. G. Nisbet, A dramatic decrease in the growth of atmospheric methane in the northern hemisphere during 1992, *Geophys. Res. Lett.*, *21*, 45–48, 1994.

Duncan, B. N., R. V. Martin, A. C. Staudt, R. Yevich, and J. A. Logan, Interannual and seasonal variability of biomass burning emission constrained by satellite observations, *J. Geophys. Res.*, *108*(D2), 4100, doi:10.1029/2002JD002378, 2003.

Feely, R. A., R. Wanninkhof, T. Takahashi, and P. Tans, Influence of El Niño on the equatorial Pacific contribution to atmospheric CO_2 accumulation, *Nature*, *398*, 597–601, 1999.

Fu, Q., P. Yang, and W. B. Sun, An accurate parameterization of the infrared radiative properties of cirrus clouds for climate models, *J. Clim.*, *11*, 2223–2237, 1998.

Garand, L., et al., Radiance and Jacobian intercomparison of radiative transfer models applied to HIRS and AMSU channels, *J. Geophys. Res.*, *106*, 24,017–24,031, 2001.

GLOBALVIEW-CO_2, *Cooperative Atmospheric Data Integration Project-Carbon Dioxide*, [CD-ROM], Clim. Monit. and Diagnostics Lab., NOAA, Boulder, Colo., 1999.

Hartmann, D. L., J. R. Holton, and Q. Fu, The heat balance of the tropical tropopause, cirrus, and stratospheric dehydration, *Geophys. Res. Lett.*, *28*, 1969–1972, 2001.

Intergovernmental Panel on Climate Change (IPCC), *Climate Change 1995: Contribution of Working Group I to the Second Assessment Report of the Intergovernmental Panel on Climate Change*, 572 pp., Cambridge Univ. Press, New York, 1995.

Jones, C. D., M. Collins, P. M. Cox, and S. A. Spall, The carbon cycle response to ENSO: A coupled climate-carbon cycle model study, *J. Clim.*, *14*, 4113–4129, 2001.

Keeling, C. D., T. P. Whorf, M. Wahlen, and J. van der Plicht, Interannual extremes in the rate of rise of atmospheric carbon dioxide since 1980, *Nature*, *375*, 666–670, 1995.

Kelly, G. A., and J. F. Flobert, Radiance tuning, in *Proceedings of the Fourth International TOVS Study Conference*, Igls, Austria, pp. 99– 117, Coop. Inst. for Meteorol. Satell. Stud., Univ. of Wis., Madison, 1988.

Li, D., and K. P. Shine, A 4-dimensional ozone climatology for UGAMP models, internal report 35, UK Univ. Global Atmos. Modell. Programme, NERC, Swindon, April 1995.

Masuda, K., T. Takashima, and Y. Takayama, Emissivity of pure and sea waters for the model of sea surface in the infrared window region, *Remote Sens. Environ.*, *24*, 313–329, 1988.

Matricardi, M., and R. W. Saunders, Fast radiative transfer model for simulation of infrared atmospheric sounding interferometer radiances, *Appl. Opt.*, *38*, 5679–5691, 1999.

Matsueda, H., and H. Inoue, Measurements of atmospheric CO_2 and CH_4 using a commercial airliner from 1993 to 1994, *Atmos. Environ.*, *30*, 1647–1655, 1996.

Matsueda, H., H. Y. Inoue, and M. Ishii, Aircraft observation of carbon dioxide at 8–13 km altitude over the western Pacific from 1993 to 1999, *Tellus, Ser. B*, *54*, 1–21, 2002.

Nakazawa, T., K. Miyashita, S. Aoki, and M. Tanaka, Temporal and spatial variations of upper tropospheric and lower stratospheric carbon dioxide, *Tellus, Ser. B*, *43*, 106–117, 1991.

Nakazawa, T., S. Murayama, K. Miyashita, S. Aoki, and M. Tanaka, Longitudinally different variations of lower tropospheric carbon dioxide concentrations over the North Pacific ocean, *Tellus, Ser. B*, *44*, 161–172, 1992.

Rayner, P. J., and D. M. O'Brien, The utility of remotely sensed CO_2 concentration data in surface source inversions, *Geophys. Res. Lett.*, *28*, 175–178, 2001.

Rayner, P. J., I. G. Enting, R. J. Francey, and R. Langenfels, Reconstructing the recent carbon cycle from atmospheric CO_2, d13C and O2/N2 observations, *Tellus, Ser. B*, *51*, 213–232, 1999.

Rumelhart, D. E., G. E. Hinton, and R. J. Williams, Learning internal representations by error propagation, in *Parallel Distributed Processing: Explorations in the Macrostructure of Cognition*, vol. 1, edited by D. E. Rumelhart and McClelland, pp. 318–362, MIT Press, Cambridge, Mass., 1986.

Schimel, D. S., J. Mellilo, H. Tian, and A. D. McGuire, Contribution of increasing CO_2 and climate to carbon storage by ecosystems in the United States, *Science*, *287*, 2004–2006, 2000.

Scott, N. A., and A. Chédin, A fast line-by-line method for atmospheric absorption computation: The Automatized Atmospheric Absorption Atlas, *J. Appl. Meteorol.*, *20*, 801–812, 1981.

Scott, N. A., et al., Characteristics of the TOVS Pathfinder Path-B dataset, *Bull. Am. Meteorol. Soc.*, *80*, 2679–2701, 1999.

Smith, W. L., H. M. Woolf, C. M. Hayden, D. Q. Wark, and L. M. McMillin, The TIROS-N operational vertical sounder, *Bull. Am. Meteorol. Soc.*, *60*, 1177–1187, 1979.

Stubenrauch, C. J., N. A. Scott, and A. Chédin, Cloud field identification for Earth radiation budget studies. Part 1: Cloud field classification using HIRS-MSU sounder measurements, *J. Appl. Meteorol.*, *35*, 416–427, 1996.

Stubenrauch, C. J., W. B. Rossow, F. Cheruy, A. Chedin, and N. A. Scott, Clouds as seen by satellite sounders (3I) and imagers (ISCCP). Part I: Evaluation of cloud parameters, *J. Clim.*, *12*, 2189–2213, 1999.

Uddstrom, M. J., and L. M. McMillin, System noise in the NESDIS TOVS forward model. Part I: Specifications, *J. Appl. Meteorol.*, *33*, 919–938, 1994.

Wahiche, C., N. A. Scott, and A. Chédin, Cloud detection and cloud parameters retrieval from the satellites of the TIROS-N series, *Ann. Geophys., Ser. B*, *4*(2), 207–222, 1986.

Wang, P. H., P. Minnis, M. P. McCormick, G. S. Kent, G. K. Yue, D. F. Young, and K. M. Skeens, A study of the vertical structure of tropical (20°S–20°N) optically thin clouds from SAGE II observations, *Atmos. Res.*, *47–48*, 599–614, 1998.

Winker, D. M., and C. R. Trepte, Laminar cirrus observed near the tropical tropopause by LITE, *Geophys. Res. Lett.*, *25*, 3351–3354, 1998.

Wofsy, S. C., R. C. Hariss, and W. A. Kaplan, Carbon dioxide in the atmosphere over the Amazon basin, *J. Geophys. Res.*, *93*, 1377–1387, 1988.

R. Armante, A. Chédin, C. Crevoisier, N. A. Scott, and S. Serrar, Laboratoire de Météorologie Dynamique, Institut Pierre-Simon Laplace, Ecole Polytechnique, F-91128 Palaiseau, France. (armante@lmd.polytechnique.fr; chedin@lmd.polytechnique.fr; crevoisier@lmd.polytechnique.fr; scott@lmd.polytechnique.fr; serrar@lmd.polytechnique.fr)